Theoretical and Applied Climatology (2022) 149:1277–1295
https://doi.org/10.1007/s00704-022-04108-2

ORIGINAL PAPER

Delineation of urban expansion and drought-prone areas using vegetation conditions and other geospatial indices

Bijay Halder[1] · Tiyasha Tiyasha[2] · Shamsuddin Shahid[3] · Zaher Mundher Yaseen[4,5,6]

Received: 15 February 2022 / Accepted: 22 May 2022 / Published online: 4 June 2022

Abstract

Drought is a dominant climatic feature in arid and semiarid regions. Climate change, temperature variability, and anthropogenic activities caused an increase in agricultural droughts in many regions. Investigation of drought dynamics is important for innovative planning and management of natural resources in drought-prone areas. Remote sensing indices and earth observational datasets were used in this study to investigate droughts in the Bikaner city of Rajasthan, India. Vegetation condition index (VCI), temperature condition index (TCI), and vegetation health index (VHI), estimated from multitemporal Landsat datasets, were used for monitoring the drought-prone areas. Land use land cover (LULC) map, normalized difference vegetation index (NDVI), and surface temperature were also calculated for monitoring the decadal changes in surface features. The results showed that barren lands decreased from around 162.75 to 79.59 km^2. The annual average temperature increased by 0.72 °C, while agricultural land increased by 33.83 km^2 during 1990–2020. There was a gradual increase in droughts, but the increase was more in recent years than in the early period. The climatic condition revealed from VCI, TCI, and NDVI maps indicated most of the Bikaner city is prone to moderate and extreme droughts. The study indicates the need for VCI-based real-time drought monitoring for drought management.

Keywords Drought monitoring · Vegetation condition index (VCI) · Temperature condition index (TCI) · Land alteration · Disaster management

1 Introduction

Global climatic conditions and environmental disturbances influence the Earth's surface processes, trigger land degradation, water shortage, vegetated land losses, thermal variation, drought, and many other ecological phenomena. Among them, droughts are the most devastating natural phenomena that affect all other processes (Liu and Kogan 1996; Mutowo and Chikodzi 2014; Sanikhani et al. 2019; Armanuos et al. 2021; Danandeh Mehr and Akdegirmen 2021; Hadri et al. 2021; Halder et al. 2021a, b; Mehr and Akdegirmen 2021). The droughts can be categorized into four classes, agronomic, hydrological, socioeconomic, and meteorological (Shahabfar et al. 2012; Ji et al. 2018; Aitkenhead et al. 2021). Agricultural droughts happen due to low precipitation, soil moisture deficiency, and vegetation losses

✉ Zaher Mundher Yaseen
yaseen@ukm.edu.my

Bijay Halder
halder06bijay@gmail.com

Tiyasha Tiyasha
tiyasha.st@tdtu.edu.vn

Shamsuddin Shahid
sshahid@utm.my

1 Department of Remote Sensing and GIS, Vidyasagar University, Midnapore, India

2 Faculty of Civil Engineering, Ton Duc Thang University, Ho Chi Minh City, Vietnam

3 School of Civil Engineering, Faculty of Engineering, Universiti Teknologi Malaysia (UTM), Johor Bahru 81310, Malaysia

5 Department of Earth Sciences and Environment, Faculty of Science and Technology, Universiti Kebangsaan Malaysia, Bangi 43600, Selangor, Malaysia

4 USQ's Advanced Data Analytics Research Group, School of Mathematics Physics and Computing, University of Southern Queensland, Queensland 4350, Australia

6 New era and Development in Civil Engineering Research Group, Scientific Research Center, Al-Ayen University, Thi-Qar 64001, Iraq

(Quiring and Ganesh 2010; Rhee et al. 2010; Jiao et al. 2019; Kulkarni et al. 2020; Aitkenhead et al. 2021). The previous studies were noted that the agricultural droughts are the consequence of longer meteorological droughts (Quiring and Ganesh 2010; Strzepek et al. 2010; Hazaymeh and Hassan 2016; Liu et al. 2016; Sur et al. 2019; Jiao et al. 2019; Kulkarni et al. 2020; Szewczak et al. 2020; Aitkenhead et al. 2021; Hadri et al. 2021; Han et al. 2021). The remote sensing and ground observational datasets are generally used to monitor agricultural droughts. Vegetation and temperature indices derived from remote sensing data are more useful for investigating the agricultural drought-prone area (Mutowo & Chikodzi 2014; Shen et al. 2019; West et al. 2019; Qutbudin et al. 2019). Monitoring agricultural droughts using remote sensing data becomes important for mitigating droughts impacts, particularly in climate change (Liu & Kogan 1996; Voogt and Oke 2003; Mallick et al. 2020). Such assessment is especially important for countries where the economy largely depends on agriculture (Wang et al. 2001; Quiring and Ganesh 2010). Water area and rainfall of the location is also indicates the ecological condition of Earth's surface (Abduallah et al. 2021; Khaleefa and Kamel 2021; Akdegirmen and Mehr 2022).

Agriculture is the backbone of the Indian economy. A major portion of the land in the country is used for agricultural purposes. The country experiences frequent drought due to large precipitation and temperature variability and loss of soil moisture. A study showed that nearly 50% of the Indian land is prone to severe drought (http://www.dsc.nrsc.gov.in/). Several droughts have affected the Indian subcontinent in recent history, which damaged crop production and forced conversation crop cultivation to livestock farming. Bikaner city and surrounding areas in India's semiarid northwest Rajasthan state have a long history of agricultural disturbances due to severe droughts. The agricultural land development and meteorological conditions have amplified the drought calamities in Bikaner city in recent years. Besides, the climate changes in the desert areas have further aggravated the situation.

Various vegetation indices have been proposed for drought monitoring like vegetation condition index (Kogan 1995a; Liu and Kogan 1996; Quiring and Ganesh 2010), temperature condition index (Wang et al. 2001, 2018; Patel et al. 2009; Zhou et al. 2020), vegetation health index (Karnieli et al. 2006; Bento et al. 2018), mapping forest area, crop sowing dates, drought and vegetation stress, and dynamics of vegetation alteration (Beyaztas and Yaseen 2019). Among them, vegetation condition assessment based on the satellite-based normalized difference vegetation index (NDVI) is most widely used to track long-term or short-term spatiotemporal droughts (Singh et al. 2003; Kulkarni et al. 2020, Mallick et al. 2021). The NDVI indicates the short and long-term fluctuation of ecological disturbances, and thus, it is more useful for drought monitoring (Li et al. 2011; Lu et al. 2012; Ramachandra et al. 2013; Hassan et al. 2016). Among the satellite data, the Landsat data are most widely used to monitor land alteration (Amiri et al. 2009; Hassan et al. 2016; Xu et al. 2016; Falah et al. 2020; Joorabian Shooshtari et al. 2020). The NDVI and land surface temperature (LST) maps derived from Landsat have been found very useful for monitorings the drought-prone area (Pramanik and Punia 2019; Joorabian Shooshtari et al. 2020).

This study is directed to land alteration and drought-prone area identification of Bikaner city using remote sensing data. The Landsat LST, NDVI, and normalized difference built-up index (NDBI) maps are employed for assessing spatiotemporal variation of agriculture drought-prone areas. The vegetation condition index (VCI) and temperature condition index (TCI) were investigated for the temporal and spatial variation of the drought. The ERDAS IMAGINE (v2014), a geospatial data authoring system and ArcGIS (v10.8), a geographical information system, were used for investigating the land alteration, vegetation condition, and visualization of the drought-prone area. The study is important for future disaster management, agricultural planning, development, water shortage analysis, planning for droughts disaster monitoring, and climate change impact assessment in Bikaner city, Rajasthan.

2 Study area

Global climate change is influencing thermal variation, vegetation conditions, and increasing the drought in arid and semiarid regions (Tolba and Najib 2009; Ahmed 2018; Zhang et al. 2021). Many parts of the Indian subcontinent are affected by several droughts, where agricultural drought is most devastating (Tabari et al. 2011; Novotná et al. 2015). Generally, the western parts of India, Rajasthan and Madhya Pradesh, are mostly affected by several droughts in a decade. Due to erratic rainfall and stumpy vegetated land, the desert state Rajasthan is widely affected by drought. In this study, the 5th largest city of Rajasthan is taken for studying drought monitoring and land alteration from 1990 to 2020.

Bikaner city is located in northwest part of the Rajasthan state, India. The Bikaner is a desert area where the average temperature in summer is around 48 °C (Fig. 1). As per the records, the average rainfall is 6.2 to 92.5 mm in July, which receives the highest rainfall. Similarly, the recorded average relative humidity is highest in month of July and August i.e., between17 to 45%. Bikaner, the 5th major populated city of Rajasthan, has inhabitants of 644,406, with a male and female ratio of 904/1000 as per https://censusindia.gov.in, 2011. The average elevation of the city is 242 m (794 ft.).

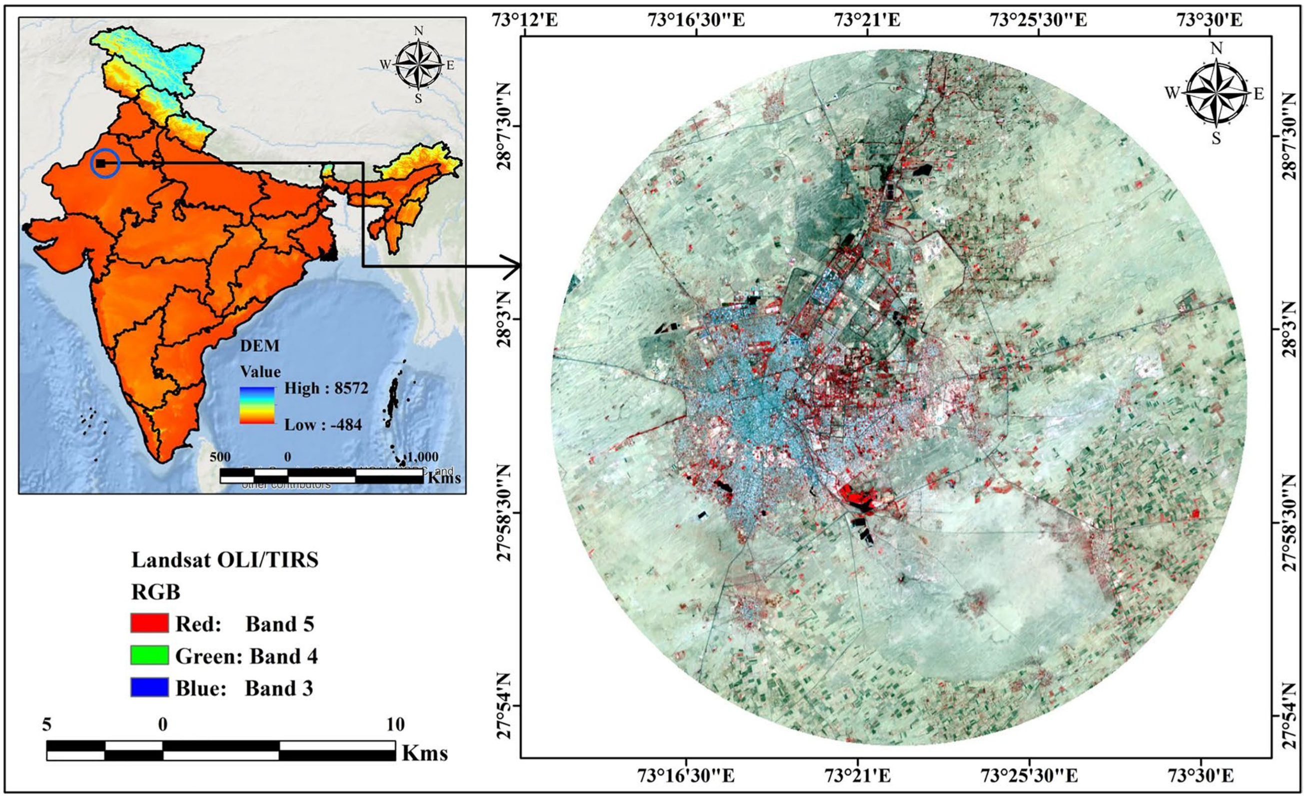

Fig. 1 Locational area of Bikaner city, Rajasthan

It is the most temperate zone of Rajasthan (https://bikaner.rajasthan.gov.in/home/dptHome/29). The total area of the study is 706.43 km^2, bounded by longitudes 73° 12′ E to 73° 31′ E and latitudes 27° 50′ N to 28° 8′ N. The study area is mostly covered by developing agricultural land in the south, south-east, and south-western.

3 Materials and method

3.1 Data used and image pre-processing

Earth observational satellite datasets were used for observing the drought and thermal deviation at Bikaner city. The four decades of data such as 1990, 2000, 2010, and 2020 were taken from Landsat 5 TM and 8 OLI/TIRS data for monitoring LULC, LST, NDVI, NDBI, and drought monitoring indices like VCI, TVI, and VHI. The data were derived from USGS earth explorer (https://earthexplorer.usgs.gov/) with 0% cloud cover (see Table 1). The chosen months were March to April since the temperature is maximum during this period. The path and row of the satellite images are 149, and 041, respectively. Table 1 shows the data acquisition and other necessary information about satellite datasets.

The satellite datasets need some geometric, atmospheric, and radiometric corrections before their processing or classification of LULC (Corner et al. 2013; Hassan et al. 2016; Somvanshi et al. 2020). FLAASH was used for atmospheric correction for a more accurate interpretation (Gao & Zhang 2009; Sejati et al. 2019). Subsequently, histogram equalization and geo-referencing were conducted for better image visualization (Meshesha et al. 2016). This follows masking, mosaic, and finally, subsetting area of interest (AOI) for

Table 1 Details of data acquisition and satellite sensors

Satellite	Sensor	Date	Path and row	Data source	Cloud cover
Landsat 5	TM	16–03-1990	149, 041	https://earthexplorer.usgs.gov/	0.00
		11–03-2000	149, 041		0.00
		24–04-2010	149, 041		0.00
Landsat 8	OLI/TIRS	18–03-2020	149, 041		0.00

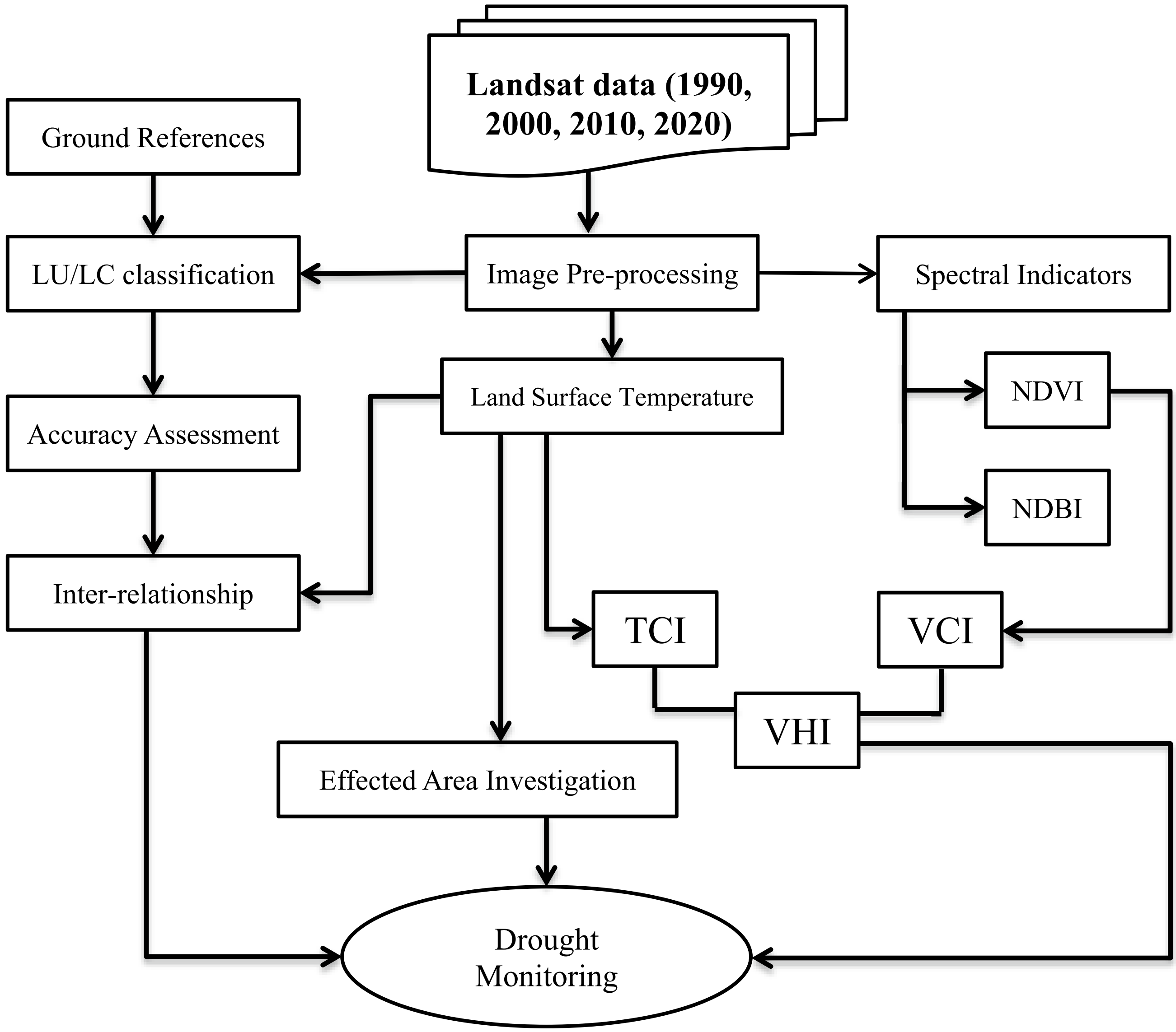

Fig. 2 Adopted methodology of this study

image classification (Fig. 2). The satellite data is affected by cloud cover, and therefore, minimum cloud cover data were derived for classification, LST calculation, and other necessary data analysis (Sobrino et al. 2004; Liu & Zhang 2011; Das et al. 2020).

3.2 Image classification and accuracy assessment

Visual interpretation is more important for land classification (Hassan et al. 2016). Therefore, the true color composite (TCC) and false-color composite (FCC) were used for monitoring the different LUCL classes of the study area (Owojori and Xie 2005; Hassan et al. 2016). After visual interpretation, different signatures were taken from the satellite datasets. The red color indicates vegetation area, and the dark black color indicates water bodies, where 10 to 55 signatures of each LULC class are obtained for classification. The supervised classification method with a maximum likelihood algorithm was used for investigating the LULC classification. The EARDAS Imagine v2014 and ArcGIS 10.8 were used for pre-processing and image classification.

The change detection, accuracy assessment, and kappa coefficient are important for post-classification techniques (Lambin and Geist 2008; Han et al. 2015; Meshesha et al. 2016). The area was calculated using count number or raster to vector conversion of each class. The formula of area calculates using count values is $Area = \left(\frac{Count*900}{1000000}\right)$ where 900 is used as the Landsat data resolution is 30 m. The monitoring LULC classes were built-up land, agricultural land, vegetation, barren land, and water body. The classification accuracy assessment and kappa coefficient calculation are important for investigating the clarity of the classification image (Falah et al. 2020) (Table 2). Google Earth data or field survey data were used for accuracy assessment. The kappa coefficient was used to idealize the classified image (Cohen 1968). The accuracy assessment and kappa coefficient are calculated using Eqs. 1 and 2.

$$OA = \left(\frac{\sum_{i=1}^{k} n_{ij}}{n} \right) \quad (1)$$

$$\mathrm{K_i} = \frac{(\text{Observed accuracy} - \text{Change accuracy})}{(1 - \text{Change accuracy})} \quad (2)$$

where n_{ij} is the oblique essentials of the error matrix, the total number of LULC classes is depicted by k, and n is the total sum of samples in the error matrix.

3.3 Investigation of geospatial indices

3.3.1 NDVI

Vegetation is the most important feature of the Earth's surface, which maintains the thermal variation, surface runoff, infiltration rate, soil erosion losses, control drought, and water level over the land surface (Li et al. 2011; Zoungrana et al. 2018). Due to urbanization, many regions are losing the vegetated land and causing thermal variations, droughts, and high evapotranspiration (Lu & Weng 2006; Jin et al. 2021). The land alteration also influences the vegetation condition. Landsat TM and OLI/TIRS datasets are widely used for monitoring the vegetation state (Sobrino et al. 2001; Li et al. 2011; Guha et al. 2018). For analyzing the vegetation health condition in Bikaner city, Rajasthan, the current study used NDVI, which can be expressed using Eq. 3.

$$NDVI = \frac{(\rho_{NIR} - \rho_R)}{(\rho_{NIR} + \rho_R)} \quad (3)$$

where NIR demonstrates the near-infrared band of Landsat images and R is the red band of satellite data. The NDVI values vary from − 1 to + 1, where 0 to − 1 indicates other LULC classes and 0 to + 1 indicates the healthy vegetation of an area.

Table 2 Scale of kappa coefficient and strength if agreement

Sl. no	Value of K	Strength of agreement
1	< 0.20	Poor
2	0.21–0.40	Fair
3	0.41–0.60	Moderate
4	0.61–0.80	Good
5	0.81–1.00	Very good

3.3.2 Introduction to NDBI

Urban expansion influences environmental degradation and localized climate change (Singh et al. 2017; Kedia et al. 2021). Population pressure has played a vital role in urban expansion and development of built-up land in Bikaner city. Urban planning is important for sustainable urban development, but overwhelming population pressure destroys the conditions (Chandler 1976; Estoque & Murayama 2017). Bikaner city has observed a vast infrastructure expansion in past decades. The NDBI is used for monitoring such urban development using Eq. 4.

$$\boldsymbol{NDBI} = \frac{(\rho_{SWIR1} - \rho_{NIR})}{(\rho_{SWIR1} + \rho_{NIR})} \quad (4)$$

where SWIR denotes shortwave infrared bands of satellite data and NIR indicates near-infrared bands of satellite data. The NDBI value varies between − 1 and + 1. Built-up lands are the positive values, whereas negative values indicate the other land classes.

3.3.3 Retrieval of LST

The thermal variation and heat alteration of an area is influenced by land surface temperature (Sobrino et al. 2004). The Landsat 5 TM (band 6) and Landsat 8 OLI/TIRS (band 10) were utilized for monitoring the LST of Bikaner city. The Landsat TM data for 1990, 2000, 2010, and Landsat OLI/TIRS for 2020 were utilized for monitoring the LST. Landsat 8 have two thermal bands, like 10 and 11. However, due to the improbability of the band 11 for LST estimation ascending caused by the tilt of the satellite orbit (Barsi et al. 2014), it was not measured in this study. Therefore, only Landsat band 10 was used to estimate LST images in the Bikaner city.

3.3.4 LST assessment from Landsat 5 TM

For the initial stage of the LST estimation, change in the digital numbers (DN) of the thermal band of the Landsat 5 TM sensor into radiance luminance (R_{TM6}) is estimated using Eq. 5 (Sobrino et al. 2004).

$$R_{TM6} = \frac{V}{255}(R_{max} - R_{min}) + R_{min} \quad (5)$$

where V presents the computerized number (DN) of the warm band 6 of Landsat 5 TM and R_{max} indicating 1.896 (mW cm^{-2} sr^{-1}) and R_{min} donates 0.1534 (mW cm^{-2} sr^{-1}).

The further step is to convert the radiance luminance into land surface temperature and unit of Kelvin (Rajeshwari and Mani 2014; Guha et al. 2018; Halder et al. 2021a, b) using Eq. 6.

$$T_k = \frac{K_1}{\ln\left(\frac{K_2}{R_{TM6}/b} + 1\right)} \tag{6}$$

where K_1 and K_2 represents the pre-calibration constant obtained from the satellite metadata files ($K_1 = 1260.56K$ and $K_2 = 607.66$ mW cm^{-2} sr^{-1} μm^{-1}); b is the spectral range ($b = 1.239$ μm).

Finally, the LST in kelvin is converted to degree Celsius utilizing Eq. 7.

$$LST = T_k - 273.15 \tag{7}$$

3.3.5 LST estimation from Landsat 8 OLI/TIRS

For preparing LST maps from Landsat 8 TIRS data, the progression in the change of DNs of ground objects to spectral radiance was estimated using Eq. 8 (Rajeshwari and Mani 2014; Roy et al. 2014; Yu et al. 2014).

$$L_\lambda = \frac{L_{max} - L_{min}}{Qcal_{max} - Qcal_{min}} * \left(\mathrm{DN} - Qcal_{min}\right) + L_{min} \tag{8}$$

where L_λ addresses the top-of-atmosphere (TOA) spectral radiance in W/(m^2 sr μm), $Qcal$ denotes the quantized adjusted pixel value in digital number (DN), L_{min} and L_{max} are the minimum and maximum spectral radiance scaled to $Qcal_{min}$ and $Qcal_{max}$ correspondingly, described in W/(m^2 sr μm), where $Qcal_{min}$ and $Qcal_{max}$ denote the minimum and maximum quantized calibrated pixel value (corresponding to L_{max}) in digital number (DN) = 255.

The brightness temperature (BT) was estimated from the perception of black body radiation as shown in Eq. 9 (Barsi et al. 2014; Roy et al. 2014).

$$T_B = \frac{K_2}{\ln\left(\frac{K_1}{L_\lambda} + 1\right)} - 273.15 \tag{9}$$

where T_B demonstrates the employable satellite brightness temperature (BT) in degree Celsius, L_λ is the spectral radiance, and K_1 and K_2 are the pre-calibration consistent achieved from the satellite metadata documents.

The subsequent stage is to precise the BT using surface emissivity alteration before estimating LST (Li et al. 2011; Tepanosyanet al. 2021). Sobrino et al. (2004) technique was utilized for this purpose, which incorporates the assessment of standard deviation (m), joined soil and vegetation emissivity (n), and extent of vegetation (P_V) as determined from Eqs. 10–12. These three parameters are used to acquire the concluding surface emissivity from Eq. 13.

$$m = (\epsilon_v - \epsilon_S) - (1 - \epsilon_S)F\epsilon_v \tag{10}$$

$$n = \epsilon_S + (1 - \epsilon_S)F\epsilon_v \tag{11}$$

$$P_V = \left(\frac{NDVI - NDVI_{min}}{NDVI_{max} - NDVI_{min}}\right)^2 \tag{12}$$

$$\varepsilon = mP_V + n \tag{13}$$

where ϵ_v and ϵ_S are the vegetation and soil emissivity, and F is the figure factor (= 0.55), located in various mathematical conveyance (Sobrino et al. 2004). The worth of m and n are estimated as 0.004 and 0.986 individually (Sobrino et al. 2004). The NDVI map is coordinated using Eq. 3 as mentioned in Sect. 3.4.

The final LST map is prepared from BT and ε using Eq. 14 (Weng et al. 2004; Li et al. 2011; Estoque and Murayama 2017).

$$LST(°C) = \frac{T_B}{1 + \left(\lambda * T_B/\rho\right)\ln\varepsilon} \tag{14}$$

where λ specifies the wavelength of emitted radiance ($\lambda = 10.8$μm), $\rho = h * c/\sigma$ (1.438×10^{-2} m K), c is the velocity of light (2.998×108 m/s), σ is the Stefan Boltzmann constant (1.38×10^{-23} J/K), and h is the Planck's constant (6.625×10^{-34} J s).

3.4 Drought monitoring indices

3.4.1 VCI

The vegetation condition index (VCI), developed by Kogan (1995b), is a controlling factor of provincial dissimilar ecosystem productivities (AghaKouchak et al. 2015; Jiao et al. 2019; Aitkenhead et al. 2021). The normalization factor of VCI is calculated from the pixel-based short-term climatological and long-term ecological signal of NDVI (West et al. 2019; Han et al. 2021). The VCI index is used for monitoring the drought using climate variables. Satellite-based indices are more useful for monitoring spatial variations of droughts, whereas climatic data is used to monitor the drought's temporal distribution (Ford and Quiring 2019; Zhang et al. 2021). The drought-prone areas are indicated by the weak vegetation growth and low NDVI values, whereas less drought-prone areas are indicated by the healthy vegetation and positive NDVI values. The VCI is calculated using Eq. 15.

$$VCI = \left(\frac{NDVI - NDVI_{min}}{NDVI_{max} - NDVI_{min}} \right) \times 100 \quad (15)$$

where $NDVI_{min}$ and $NDVI_{max}$ are calculated from long term satellite data using NIR and Red bands. The healthy vegetations indicate a low drought-prone area, and less vegetation areas denote a high drought area. The VCI values are calculated in %, where 0 to 100% indicates no drought.

3.4.2 TCI

Climate change is the most important factor for thermal variation and methodological conditions. The thermal variation is also influenced by the vegetation of an area, where arid and semiarid regions are mostly affected by heat variation due to desert locations (Masoudi 2021). Kogan (1995a) established TCI for monitoring the spatial variation of droughts using satellite images. The TCI is almost the same as VCI, where maximum and minimum values of LST are used. The TCI is calculated following Eq. 16.

$$TCI = \left(\frac{LST_{max} - LST}{LST_{max} - LST_{min}} \right) \times 100 \quad (16)$$

where LST_{min} and LST_{max} are determined from long haul satellite information utilizing thermal bands (band 6 for Landsat 5 TM and 10 for Landsat 8 OLI/TIRS). The TCI is calculated in %, where 0 to 100% indicates no drought.

3.4.3 VHI

Vegetation plays a vital role in environmental conditions and in controlling the soil's thermal variation and moisture content (Potter et al. 2001; Kamoutsis et al. 2018; Lozano-Parra et al. 2018; Rita et al 2021). The healthy vegetation enhances infiltration rate and soil moisture content. The VHI is calculated from VCI and TCI using Eq. 17.

$$\mathrm{VHI} = 0.5 \times (\mathrm{VCI} + \mathrm{TCI}) \quad (17)$$

The VHI ranges between 0 and 100. VHI higher than 50 indicates healthy vegetation.

4 Results and discussion

4.1 Land alteration investigation

Earth surface change analysis is vital for investigating climatic, anthropogenic, and meteorological disturbances. Extreme weather conditions and population pressure influence local environmental conditions and disrupt the ecosystem. In recent decades, many parts of India have observed a huge land alteration due to population pressure, where forests were converted into agricultural land, built-up land, and industrial works. Therefore, a land alteration study is important for investigating the actual scenarios of the Earth's surface changes. The four Landsat data (5 TM and 8 OLI/TIRS) information were utilized for observing the LULC maps over Bikaner city.

The results showed that the developed land was progressively expanded because of populace pressure and developed regions, 48.06 km^2 (1990), 74.86 km^2 (2000), 81.04 km^2 (2010), and 127.65 km^2 (2020) (Table 3). The average annual growth of built-up land was 2.65 km^2 due to population pressure and anthropogenic activities in Bikaner city. Vegetation areas also expanded, but they cannot be considered healthy vegetation. Figure 3 shows the LULC change and spatiotemporal variation of each LULC class. The vegetation areas were 18.98 km^2 in 1990, 12.73 km^2 in 2000, 29.44 km^2 in 2010, and 67.14 km^2 in 2020. This indicates the vegetation increased in the study area. However, healthy vegetation was not developed due to anthropogenic activities and thermal variation. The agricultural lands were increased due to food scarcity and the necessity of cropland. The agricultural land development was more in the south and south-eastern parts of the study area. The spread of agricultural lands was 0.19 km^2 in 1990, 0.62 km^2 in 2000, 13.91 km^2 in 2010, and 34.02 km^2 in 2020, where most agricultural land expansions occurred during 2010−2020. The water bodies also increased in the core area of the Bikaner city as some lakes were developed to mitigate water scarcity. The located water areas were 0.48 km^2 in 1990, 0.46 km^2 in 2000, 1.09 km^2 in 2010, and 1.65 km^2 in 2020. The thermal variation was high in the city, but built-up expansion

Table 3 Area calculation of LULC classes in different time periods

Sl. no	Class name	Area (km^2)				Area (%)			
		1990	2000	2010	2020	1990	2000	2010	2020
1	Built-up land	48.06	74.86	81.04	127.65	6.80	10.60	11.47	18.07
2	Vegetation	18.98	12.73	29.44	67.14	2.69	1.80	4.17	9.50
3	Agricultural land	0.19	0.62	13.91	34.02	0.03	0.09	1.97	4.82
4	Water body	0.48	0.46	1.09	1.65	0.07	0.07	0.15	0.23
5	Barren land	638.72	617.76	580.95	475.97	90.42	87.45	82.24	67.38
	Total area	706.43	706.43	706.43	706.43				

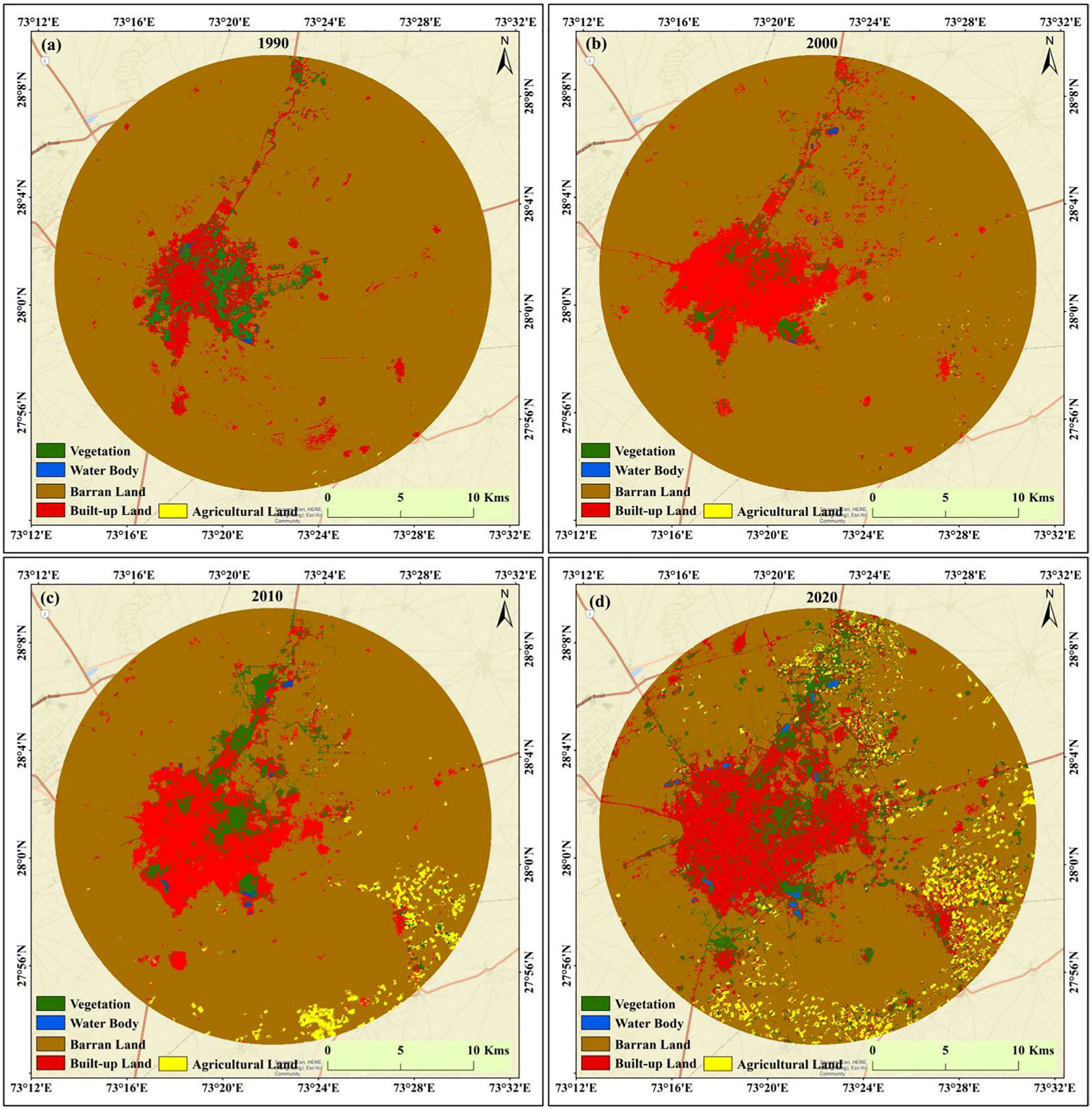

Fig. 3 LULC classes of Bikaner city of different time periods

reduced the total barren lands, 638.72 km^2 in 1990, 617.76 km^2 in 2000, 580.95 km^2 in 2010, and 475.97 km^2 in 2020. Around 162.75 km^2 of barren land was reduced due to urban expansion, agricultural land development, and expansion of vegetated lands.

Table 4 shows the changes in each LULC class of Bikaner city. The results showed that the built-up land, agricultural land, and vegetation area were increased, whereas barren land was decreased due to urban expansion and anthropogenic activities in this area. The decadal built-up land expansions were 26.8 km^2 during 1990–2000, 74.86 km^2 during 2000–2010, 46.61 km^2 during 2010–2020, and 79.59 km^2 during 1990–2020. The vegetation areas increased during 2000−2020 but decreased during 1990–2000. Figure 4 shows the total areas of classification maps and fluctuation of LULC classes in different periods. The barren lands decreased by about 20.96 km^2 during 1990–2000, 36.81 km^2 during 2000–2010, 104.98

Table 4 LULC classes loss and gain of the Bikaner city

Sl. no	Class name	Area (km^2)			
		(1990–2000)	(2000–2010)	(2010–2020)	(1990–2020)
1	Built-up land	26.8	74.86	46.61	79.59
2	Vegetation	– 6.25	16.71	37.7	48.16
3	Agricultural land	0.43	13.29	20.11	33.83
4	Water body	– 0.02	0.63	0.56	1.17
5	Barren land	– 20.96	– 36.81	– 104.98	– 162.75

km^2 during 2010–2020, and 162.75 km^2 during 1990–2020. The accuracy assessment and kappa coefficient values were within the acceptable limits. The overall accuracy was 85.75, 82.99, 84.06, and 86.86%, where kappa coefficients were 0.82, 0.79, 0.80, and 0.82 for the years 1990, 2000, 2010, and 2020, respectively. A 23.04% decrease was observed in barren land over 30 years, but that does not mean that the difference was added to forestation, rather 11.27% was added to built-up land, 6.81% to vegetation land, 4.79% to agricultural land, and 0.16% to water bodies (Table 3). There was an exponential increase in build-up land. In contrast, the increase in agricultural and water areas was rather less. This shows that authorities were less concern over the last 30 years on sustainable growth and environment-friendly development.

4.2 Topographical distribution of LST

Temperature disparity is a crucial perspective for examining the worldwide environmental change and its impacts on

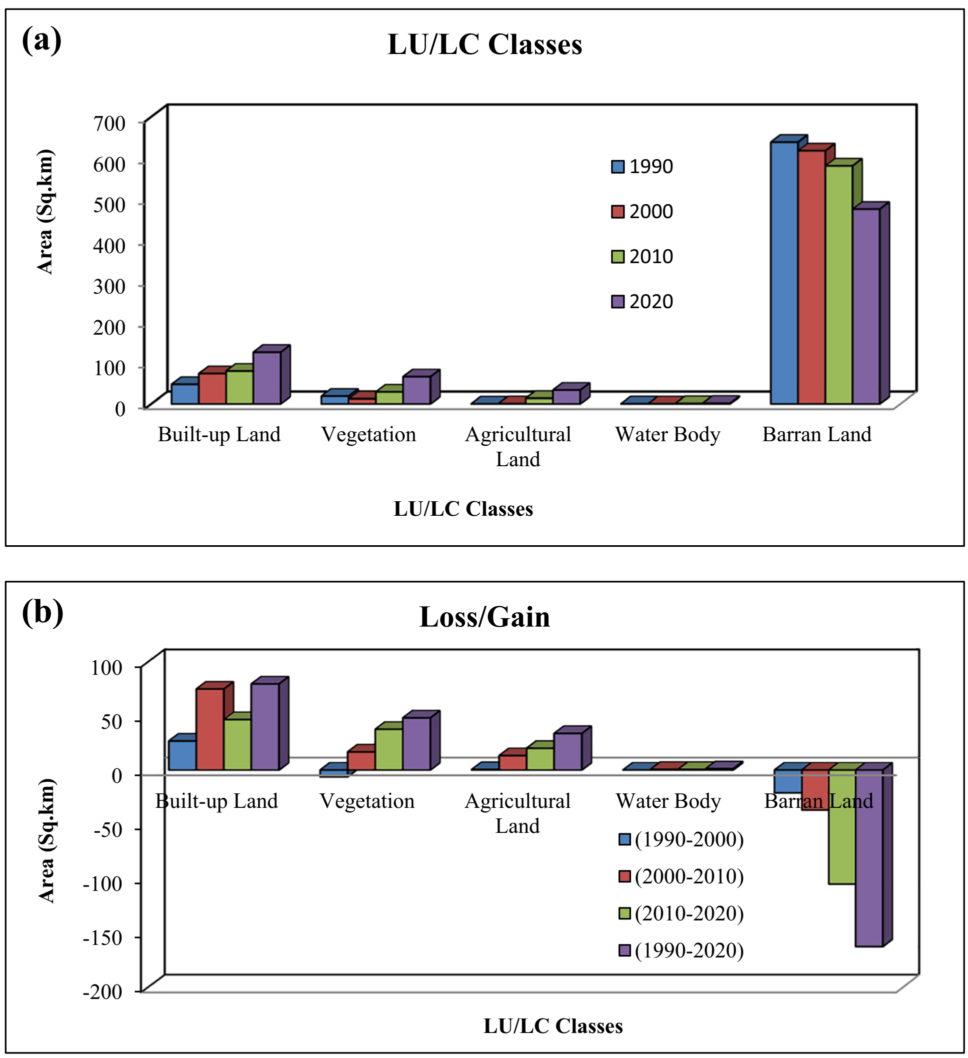

Fig. 4 Area of different LULC classes. **a** Total areas of different LULC classes. **b** Loss and gain areas of Bikaner city

the world's surface (Das et al. 2020). The high temperature influences evapotranspiration rate, vegetation health, water shortage, and declined soil moisture in the desert areas. The increasing LSTs were noticed over the years, i.e., LST was only 32.86 °C in 1990, and the populated area was rather cold with a minimum LST of 24.54 °C, whereas the LST increased to 41.45 °C during 2000 and the cooler zone was considerably decreased with increased minimum temperature to 27.93 °C. However, from 2000 to 2010, the increase in the cooler zone was observed as in Fig. 5c, where the highest temperature reached 51.49 °C, and similarly, the highest temperature reached 54.50 °C by 2020 (see Fig. 5 c and d). Moreover, LST increased over the year, but in 2010, most of the zone showed mixed temperature variation, while in 2020, only the build-up land remained cool. These conditions indicated a gradual increase in thermal discomfort. The LST was high in barren land and near agricultural lands. The annual average temperature rise was 0.86 °C during

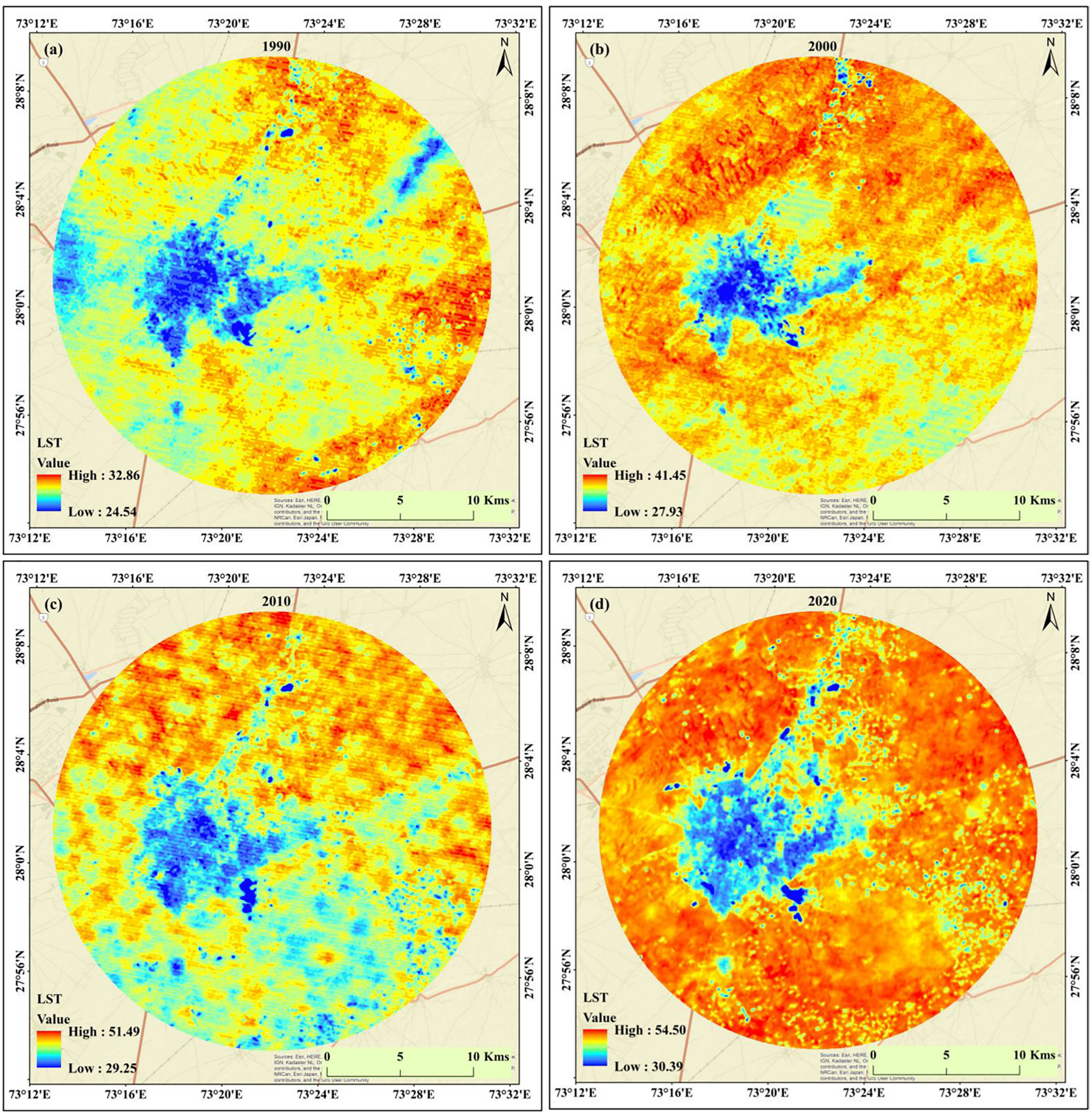

Fig. 5 LST maps of different time: **a** 1990; **b** 2000; **c** 2010; **d** 2020

Table 5 LST variation of different time periods

Sl. no	Year	LST (°C)		
		Maximum	Minimum	Average
1	1990	32.86	24.54	28.7
2	2000	41.45	27.93	34.69
3	2010	51.49	29.25	40.37
4	2020	54.5	30.39	42.44

1990–2000, 1.004 °C during 2000–2010, 0.30 °C during 2010–2020, and 0.72 °C during 1990–2020, whereas the most affected years were 2000 to 2010. The results indicate the topographical variation of LST in Bikaner city and surrounding areas. The red color indicates the high temperature, whereas the blue color indicates the low temperature. Table 5 shows the maximum, minimum, and average variations in LST in Bikaner city. The built-up land, vegetation, and water bodies had low temperatures, whereas barren land had more temperate. Moreover, the LST measure showed localized climate change where the maximum LST increase was 21.64 °C, whereas the minimum LST increase was 24.54−30.39 °C (see Table 5). Figure 5 shows that the build-up area in 2020 was cooler though the minimum LST increased by 5.85 °C. This indicates that required preventive measures and increased green coverage were neglected during urban development. The results presented in this section can help generate the TCI and VHI maps for estimating the drought-related information in Bikaner city.

4.3 Urban expansion study

The normalized difference built-up index was utilized for assessing the extension of Bikaner city. Figure 6 indicates the built-up area expansion in Bikaner city. The urban area was extended towards the north, south, and south-eastern of the city. Besides, the urbanization within the city became denser. The most noteworthy increase in NDBI were 0.04 (1990), 0.08 (2000), 0.11 (2010), and 0.30 (2020). These indicate that the built-up land expanded gradually, whereas agricultural lands also increased. The average annual NDBI value was increased by 0.008 during 1990–2020, whereas 0.019 during 2010–2020. These scenarios indicate that the expansion of the built-up lands was high during 2010−2020.

4.4 Vegetation condition examination

Vegetation is more important for regional thermal comfort and for maintaining the moisture content of the Earth's surface (Zhou et al. 2020; Halder and Bandyopadhyay 2022). NDVI was used for monitoring the vegetation health of Bikaner city for over three decades. The results showed that the vegetation of many parts of the city was affected during different periods (Fig. 7). The green color on the map indicates the healthy vegetation, whereas the blue indicates the barren land. The highest NDVI was 0.33 in 1990, 0.26 in 2000, 0.22 in 2010, and 0.16 in 2020. The NDVI maps indicate a gradual decrease in vegetation health. The areas with agricultural lands were more vegetated. The average annual vegetation health was 0.007 during 1990–200, 0.004 during 2000–2010, 0.006 during 2010–2020, and 0.006 during 1990–2020. Figure 6 shows that most of the vegetation concentration was in the middle western part, and it was further increasing towards the north in 1990 but started to expand towards the northeast in 2000. By 2020, expansion was scattered and occupied mostly barren lands. This observation can be compared with LULC class distribution, presented in Fig. 3, where yellow dots are the agricultural land and green dots are the vegetation. The comparison of LULC and NDVI maps helped to understand that agricultural land increased considerably and mostly towards west and south barren-land areas. However, it should be noted that NDVI categorizes agricultural land as vegetation, and thus, it is important for the domain expert to analyze both.

4.5 Drought analysis using VCI and TCI

The vegetation indices are more important for drought and ecological disturbances analysis. Therefore, NDVI, VCI, and VHI were used to monitor the spatiotemporal variations of the drought indices. The NDVI (Fig. 7) was less than 0.45, indicating low vegetation almost every year and high drought frequently. The spatiotemporal changes in VCI are presented in Fig. 8, where the area is classified into five regions, no dry spell, light dry spell, moderate dry spell, serious dry season, and extreme dry season. The blue color in the figure indicates no drought, whereas the brown color indicates extreme droughts. The minimum and maximum NDVI values were used for monitoring the VCI values. The results showed fewer extreme droughts between 1990 and 2000, whereas more extreme droughts between 2010 and 2020. This indicates the deterioration of vegetation health and more ecological disturbances in this area over time. No drought was observed in the central part due to urban areas, but the rest of the areas are prone to moderate to extreme droughts. These maps can be helpful for planners, disaster management, and policymaking for future planning.

Figure 9 shows the TCI calculated from LST. The March and April of every year were considered for estimating drought variability. The red color in the figure indicates extreme drought, whereas the green color indicates no drought. The figure shows that most of the parts are prone to severe to extreme droughts. The decades 2000, 2010, and 2020 were mostly drought-prone, whereas 1990 was

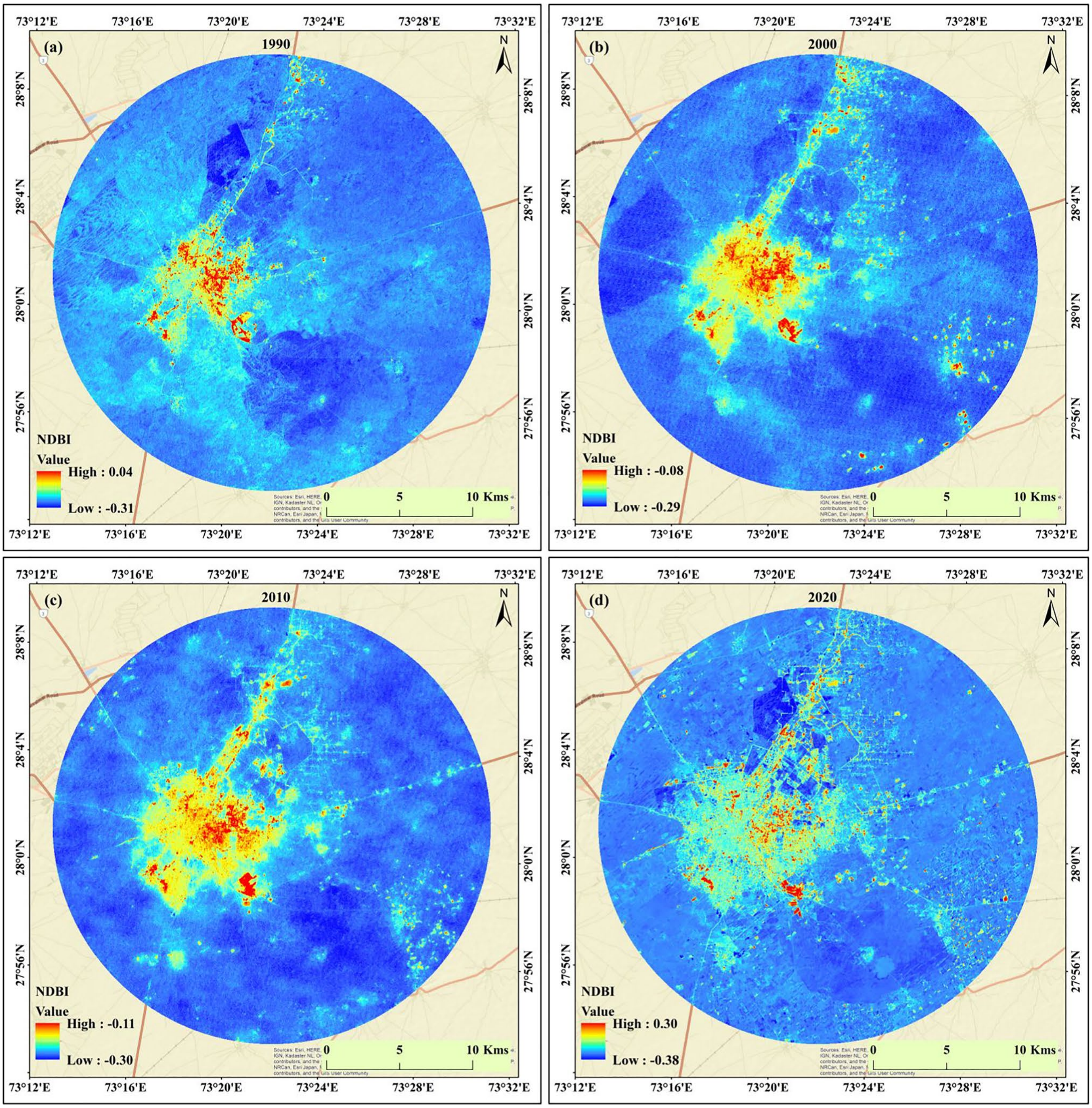

Fig. 6 NDBI maps of different time: **a** 1990; **b** 2000; **c** 2010; **d** 2020

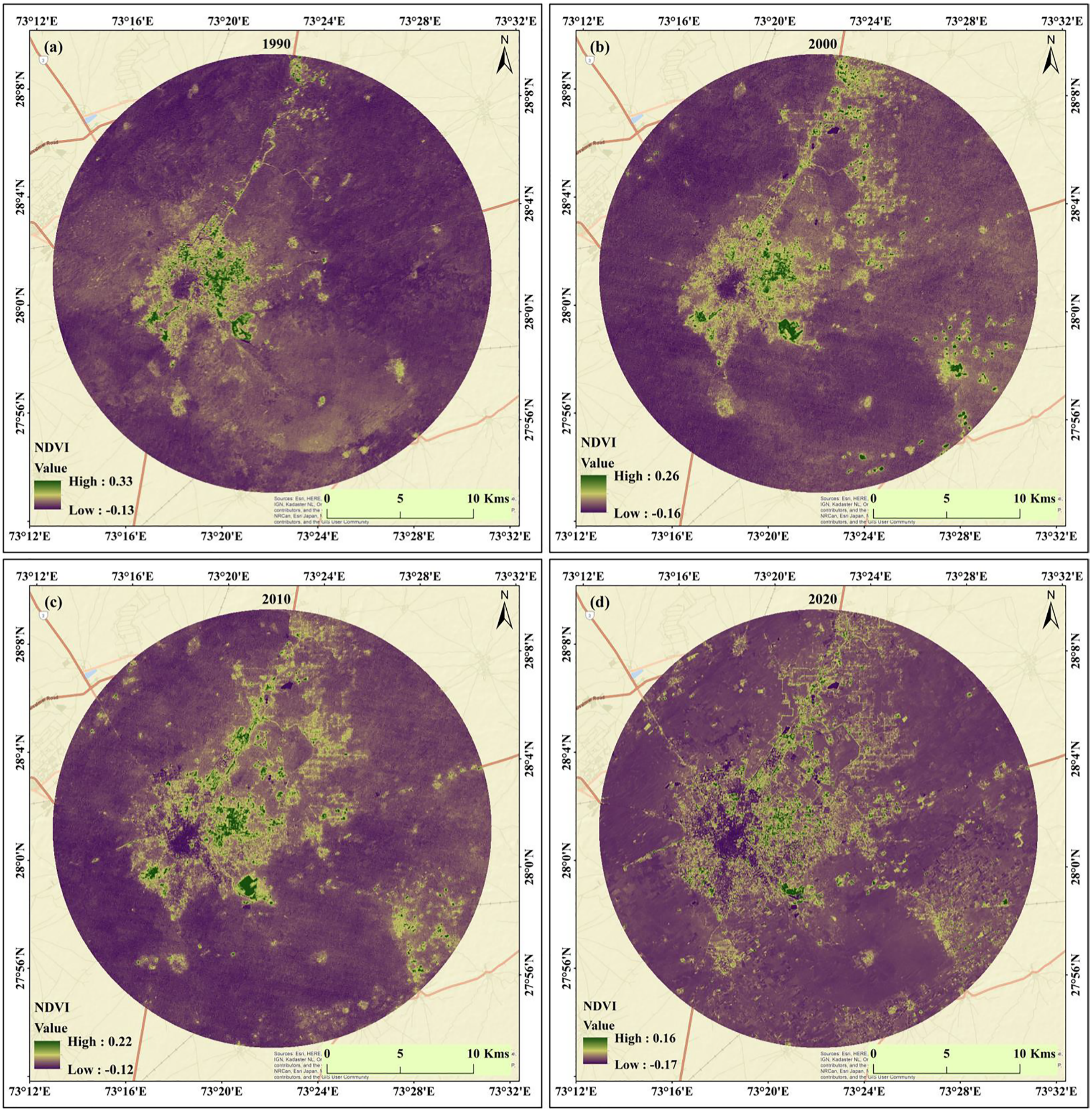

Fig. 7 NDVI maps of different time: **a** 1990; **b** 2000; **c** 2010; **d** 2020

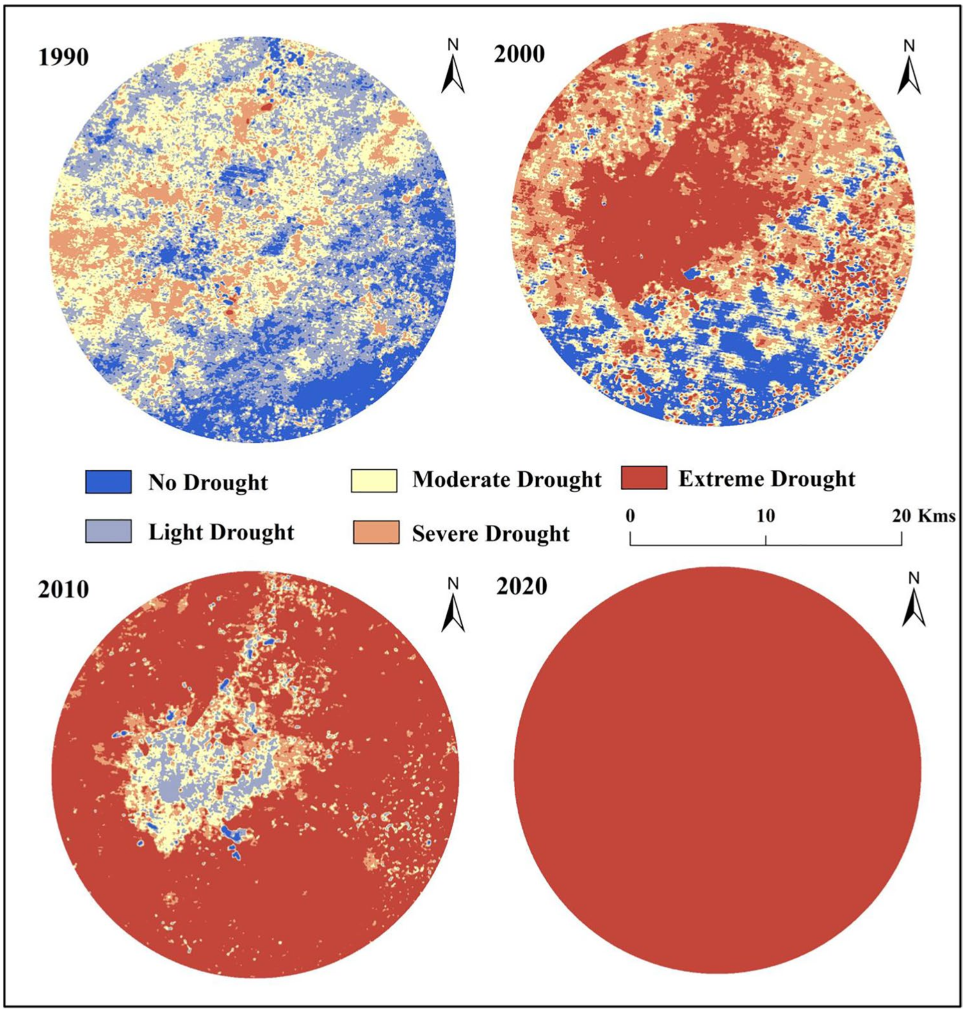

Fig. 8 Vegetation condition index (VCI) of different time periods

less drought-prone. Figures 8 and 9 indicate the worsening drought condition in the study area. In 2020, there was hardly any point without extreme drought. The results indicate severe implications not only for humans but also for animals and ecology. The condition can deteriorate in the near future if no measures are taken.

4.6 Investigating the vegetation health index

Vegetation health is another useful metric for investigating drought-prone areas. The VHI was estimated from VCI and TCI using Eq. 17. The VHI of more than 50 indicates normal to low drought, and below 50 indicates normal to high drought. Figure 10 indicates the variation of the VHI in different periods, where the most affected year was 2010 and 2020. The most affected areas were agricultural land and barren land, where built-up land, vegetation, and water bodies were low drought-prone areas.

This study is more helpful for the future planning, development, and management of Bikaner city. However, a more detailed study is necessary for awareness, planning, and future development of the study area. The land alteration, LST variation, geospatial indicates, VCI, TCI, and VHI values are useful for investigating the earth surface changes and environmental issues in Bikaner city, but some limitations are there, like the necessity of ground-level detail investigation, hydrological and meteorological drought analysis using standardized precipitation index, effective drought index, and monthly drought analysis.

5 Conclusions

Drought frequency is increasing in many parts of India, causing crop damage, soil fertility losses, water shortage, and environmental degradation. These have severely

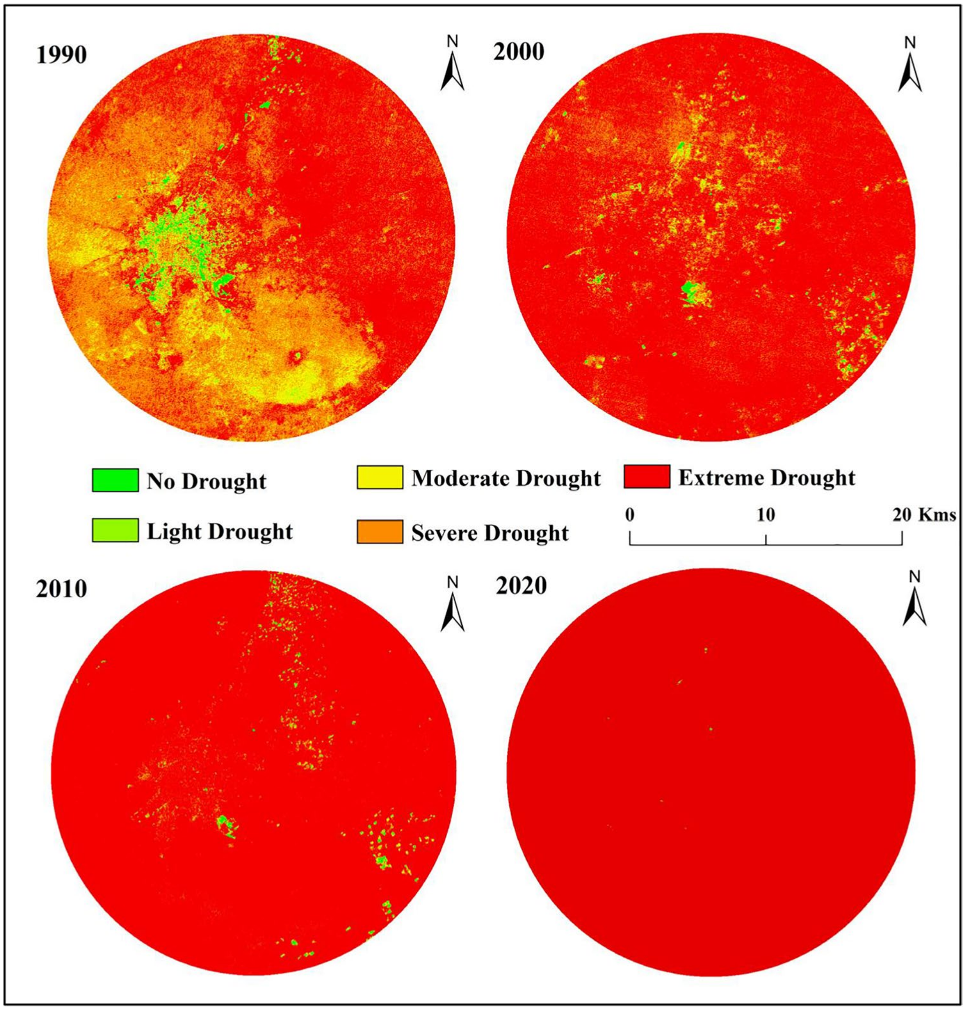

Fig. 9 Temperature condition index (TCI) of different time periods

affected socioeconomic development and people's healthy life. The desert area of Bikaner is mostly affected by thermal variations, water scarcity, and low rainfall. The annual average rainfall is around 45–50 mm, whereas in July, the highest rainfall month, it is around 90.2 mm. In the arid and semiarid regions, lands have been gradually converted to drylands due to climate change and ecological disturbances. This study assessed the land modification, thermal variability, vegetated land change, and metropolitan development in Bikaner city. The NDVI and LST-based VCI, TCI, and VHI indices were used. The study showed that the developed land, rural land, vegetation, and water bodies were expanded by 79.59, 48.16, 33.83, and 1.17 km^2, respectively. The infertile land diminished by 20.96 km^2 during 1990−2000, 36.81 km^2 during 2000−2010, and 104.98 km^2 during 2010−2020.

Drought monitoring is a vital research aspect for assessing agricultural productivities, water shortage, and local climatic conditions. Bikaner city is mostly affected by meteorological droughts due to erratic rainfall, high-temperature variations, and high evapotranspiration. The future works needed for sustainable development in the area like the future drought projections, water shortage analysis, agricultural productivities analysis, urban sprawl estimation, urban planning investigation, and thermal comfort estimation. The results presented in this paper can benefit planners and developers for drought monitoring and management, agricultural productivities investigation, and other stakeholders for sustainable development planning of the area. Likewise, the techniques presented in this study are valuable for other relevant exploration with and without reasonable adjustment.

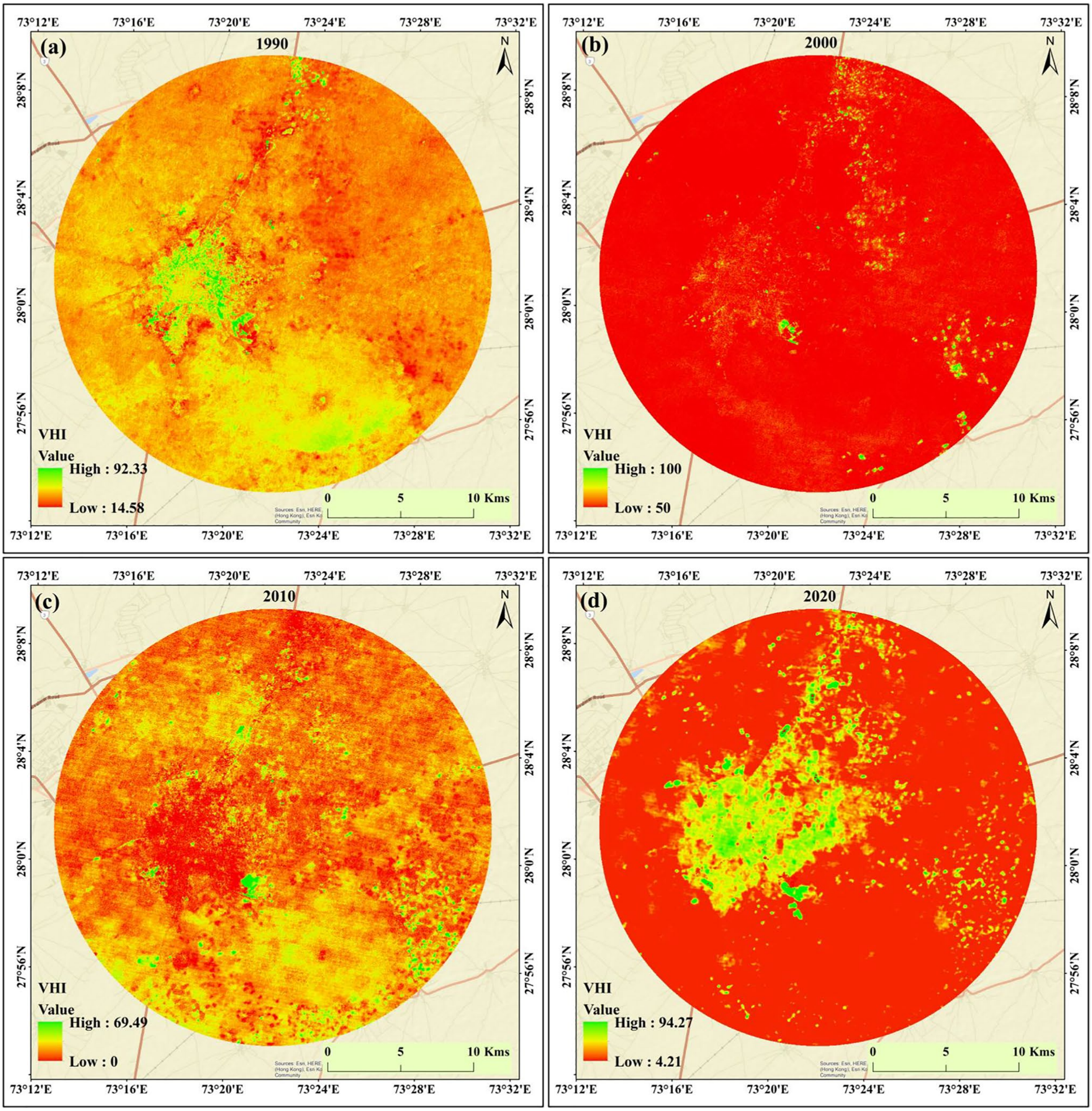

Fig. 10 Vegetation health index (VHI) of different time periods: **a** 1990; **b** 2000; **c** 2010; **d** 2020

Acknowledgements The authors acknowledge the support provided by Al-Ayen University.

Author contribution Bijay Halder: data curation; formal analysis; methodology; investigation; visualization; writing—original draft, review and editing draft preparation; resources; software. Tiyasha Tiyasha: investigation; visualization; writing—original draft, review and editing draft preparation. Shamsuddin Shahid: supervision; validation; investigation; visualization; writing—original draft, review and editing draft preparation. Zaher Mundher Yaseen: supervision, conceptualization; project administration; writing—review and editing.

Declarations

Ethical approval The study is conducted considering the ethical manner advised by the journal.

Consent to participate Not applicable.

Consent to publish All authors approve consent to publish the paper.

Conflict of interest The authors declare no competing interests.

Availability of data and materials Data will be supplied upon request to the corresponding author.

References

Abduallah RM, Alosta MM, Bahri S (2021) On the analysis and assessment of large concrete dam using finite element approach. Knowledge-Based Eng Sci 2(3):23–33

AghaKouchak A, Farahmand A, Melton FS, Teixeira J, Anderson MC, Wardlow BD, Hain CR (2015) Remote sensing of drought: progress, challenges and opportunities. Rev Geophys 53(2):452–480

Ahmed S (2018) Assessment of urban heat islands and impact of climate change on socioeconomic over Suez Governorate using remote sensing and GIS techniques. Egypt J Remote Sens Space Sci 21(1):15–25

Aitkenhead I, Kuleshov Y, Watkins AB, Bhardwaj J, Asghari A (2021) Assessing agricultural drought management strategies in the Northern Murray-Darling Basin. Nat Hazards 109(2):1425–1455

Akdegirmen O & Mehr AD. (2022). Stormwater Drainage Impact of Impervious Structures on Surrounding Soil.

Amiri R, Weng Q, Alimohammadi A, Alavipanah SK (2009) Spatial–temporal dynamics of land surface temperature in relation to fractional vegetation cover and land use/cover in the Tabriz urban area. Iran Remote Sens Environ 113(12):2606–2617. https://doi.org/10.1016/j.rse.2009.07.021

Armanuos A, Ahmed K, SanusiShiru M, Jamei M (2021) impact of increasing pumping discharge on groundwater level in the Nile Delta aquifer. Egypt Knowledge-Based Eng Sci 2(2):13–23. https://doi.org/10.51526/kbes.2021.2.2.13-23

Barsi JA, Schott JR, Hook SJ, Raqueno NG, Markham BL, Radocinski RG (2014) Landsat-8 thermal infrared sensor (TIRS) vicarious radiometric calibration. Remote Sensing 6(11):11607–11626. https://doi.org/10.3390/rs61111607

Bento VA, Trigo IF, Gouveia CM, DaCamara CC (2018) Contribution of land surface temperature (TCI) to vegetation health index: a comparative study using clear sky and all-weather climate data records. Remote Sens 10(9):1324

Beyaztas U, Yaseen ZM (2019) Drought interval simulation using functional data analysis. J Hydrol 579:124141

Bougara H, Hamed KB, Borgemeister C, Tischbein B, Kumar N (2020) Analyzing trend and variability of rainfall in the Tafna basin (Northwestern Algeria). Atmosphere 11(4):347

Chakraborty T, Hsu A, Manya D, Sheriff G (2020) A spatially explicit surface urban heat island database for the United States: characterization, uncertainties, and possible applications. ISPRS J Photogramm Remote Sens 168:74–88. https://doi.org/10.1016/j.isprsjprs.2020.07.021

Chandler TJ. (1976). Urban climatology and urban planning. Geographical J, 57-59. https://doi.org/10.2307/1796024

Cohen J. (1968). "Weighted kappa: nominal scale agreement provision for scaled disagreement or partial credit." *Psychological Bulletin*.

Corner RJ, Dewan AM, Chakma S (2013) Monitoring and prediction of land-use and land-cover (LULC) change. In: Dhaka megacity. Springer, Dordrecht, pp 75–97. https://doi.org/10.1007/978-94-007-6735-5_5

Costello A, Abbas M, Allen A, Ball S, Bell S, Bellamy R, ... & Patterson C. (2009). Managing the health effects of climate change: lancet and University College London Institute for Global Health Commission. *The lancet*, *373*(9676), 1693-1733

DanandehMehr A, Akdegirmen O (2021) Estimation of urban imperviousness and its impacts on flashfloods in Gazipaşa. Turkey. Knowledge-Based Eng Sci 2(1):9–17. https://doi.org/10.51526/kbes.2021.2.1.9-17

Das P, Vamsi KS, Zhenke Z (2020) Decadal variation of the land surface temperatures (LST) and urban heat island (UHI) over Kolkata City projected using MODIS and ERA-Interim datasets. Aerosol Sci Eng 4(3):200–209

Estoque RC, Murayama Y (2017) Monitoring surface urban heat island formation in a tropical mountain city using Landsat data (1987–2015). ISPRS J Photogramm Remote Sens 133:18–29. https://doi.org/10.1016/j.isprsjprs.2017.09.008

Falah N, Karimi A, Harandi AT (2020) Urban growth modeling using cellular automata model and AHP (case study: Qazvin city). Model Earth Syst Environ 6(1):235–248. https://doi.org/10.1007/s40808-019-00674-z

Ford TW, Quiring SM (2019) Comparison of contemporary in situ, model, and satellite remote sensing soil moisture with a focus on drought monitoring. Water Resour Res 55(2):1565–1582

Gao Y, Zhang W (2009) LULC classification and topographic correction of Landsat-7 ETM+ imagery in the Yangjia River Watershed: the influence of DEM resolution. Sensors 9(3):1980–1995

Giorgi F, Lionello P (2008) Climate change projections for the Mediterranean region. Global Planet Change 63(2–3):90–104

Guha S, Govil H, Dey A, Gill N (2018) Analytical study of land surface temperature with NDVI and NDBI using Landsat 8 OLI and TIRS data in Florence and Naples city. Italy Eur J Remote Sens 51(1):667–678

Hadri A, Saidi MEM, Boudhar A (2021) Multiscale drought monitoring and comparison using remote sensing in a Mediterranean arid region: a case study from west-central Morocco. Arab J Geosci 14(2):1–18

Halder B, Bandyopadhyay J (2022) Delineation of geospatial indices based water bodies' and vegetation change mapping using Sentinel-2 imagery in Canning blocks of south 24 parganas district, India. Remote Sens Appl: Soc Environ 25:100688. https://doi.org/10.1016/J.RSASE.2021.100688

Halder B, Bandyopadhyay J, Banik P (2021a) Monitoring the effect of urban development on urban heat island based on remote sensing and geospatial approach in Kolkata and adjacent areas. India Sustain Cities Soc 74:103186

Halder B, Haghbin M, Farooque AA (2021b) An assessment of urban expansion impacts on land transformation of Rajpur-Sonarpur municipality. Knowledge-Based Eng Sci 2(3):34–53. https://doi.org/10.51526/kbes.2021.2.3.34-53

Hamlaoui-Moulai L, Mesbah M, Souag-Gamane D, Medjerab A (2013) Detecting hydro-climatic change using spatiotemporal analysis of rainfall time series in Western Algeria. Nat Hazards 65(3):1293–1311

Han H, Bai J, Yan J, Yang H, Ma G (2021) A combined drought monitoring index based on multi-sensor remote sensing data and machine learning. Geocarto Int 36(10):1161–1177

Han H, Yang C, Song J (2015) Scenario simulation and the prediction of land use and land cover change in Beijing. China Sustain 7(4):4260–4279. https://doi.org/10.3390/su7044260

Hassan Z, Shabbir R, Ahmad SS, Malik AH, Aziz N, Butt A, Erum S (2016) Dynamics of land use and land cover change (LULCC) using geospatial techniques: a case study of Islamabad Pakistan. Springerplus 5(1):1–11. https://doi.org/10.1186/s40064-016-2414-z

Hazaymeh K, Hassan QK (2016) Remote sensing of agricultural drought monitoring: a state of art review. AIMS Environ Sci 3(4):604–630

Ifatimehin OO, Ufuah ME (2006) An analysis of urban expansion and loss of vegetation cover in Lokoja, using GIS techniques. Zaria Geogr 17(1):28–36

Ji T, Li G, Yang H, Liu R, He T (2018) Comprehensive drought index as an indicator for use in drought monitoring integrating multi-source remote sensing data: a case study covering the Sichuan-Chongqing region. Int J Remote Sens 39(3):786–809

Jiao W, Tian C, Chang Q, Novick KA, Wang L (2019) A new multi-sensor integrated index for drought monitoring. Agric for Meteorol 268:74–85

Jin Z, Zhang L, Lv J, Sun X (2021) The application of geostatistical analysis and receptor model for the spatial distribution and sources of potentially toxic elements in soils. Environ Geochem Health 43(1):407–421. https://doi.org/10.1007/s10653-020-00729-6

Joorabian Shooshtari S, Silva T, Raheli Namin B, Shayesteh K (2020) Land use and cover change assessment and dynamic spatial modeling in the Ghara-su Basin, Northeastern Iran. J Indian Soc Remote Sens 48(1):81–95. https://doi.org/10.1007/s12524-019-01054-x

Kamoutsis A, Chronopoulos K, Matsoukis A (2018) Altitude and canopy cover effects on air temperature in a mountainous region of Ionian Islands. Greece Curr World Environ 13(3):292–298. https://doi.org/10.12944/CWE.13.3.03

Karnieli A, Bayasgalan M, Bayarjargal Y, Agam N, Khudulmur S, Tucker CJ (2006) Comments on the use of the vegetation health index over Mongolia. Int J Remote Sens 27(10):2017–2024

Kedia S, Bhakare SP, Dwivedi AK, Islam S, Kaginalkar A (2021) Estimates of change in surface meteorology and urban heat island over northwest India: Impact of urbanization. Urban Climate 36:100782

Khaleefa O, Kamel AH (2021) On the evaluation of water quality index: Case study of Euphrates river. Iraq Knowledge-Based Eng Sci 2(2):35–43

Kim SW, Brown RD (2021) Urban heat island (UHI) intensity and magnitude estimations: A systematic literature review. Sci Total Environ 779:146389

Kogan FN (1995a) Application of vegetation index and brightness temperature for drought detection. Adv Space Res 15(11):91–100

Kogan FN (1995b) Droughts of the late 1980s in the United States as derived from NOAA polar-orbiting satellite data. Bull Am Meteor Soc 76(5):655–668

Kulkarni SS, Wardlow BD, Bayissa YA, Tadesse T, Svoboda MD, Gedam SS (2020) Developing a remote sensing-based combined drought indicator approach for agricultural drought monitoring over Marathwada. India Remote Sens 12(13):2091

Lambin EF & Geist HJ. (Eds.). (2008). *Land-use and land-cover change: local processes and global impacts*. Springer Science & Business Media.

Li J, Song C, Cao L, Zhu F, Meng X, Wu J (2011) Impacts of landscape structure on surface urban heat islands: a case study of Shanghai. China Remote Sens Environ 115(12):3249–3263. https://doi.org/10.1016/j.rse.2011.07.008

Liu WT, Kogan FN (1996) Monitoring regional drought using the vegetation condition index. Int J Remote Sens 17(14):2761–2782

Liu L, Zhang Y (2011) Urban heat island analysis using the Landsat TM data and ASTER data: A case study in Hong Kong. Remote Sens 3(7):1535–1552. https://doi.org/10.3390/rs3071535

Liu X, Zhu X, Pan Y, Li S, Liu Y, Ma Y (2016) Agricultural drought monitoring: Progress, challenges, and prospects. J Geog Sci 26(6):750–767

Lozano-Parra J, Pulido M, Fondón CL, Schnabel S (2018) How do soil moisture and vegetation covers influence soil temperature in drylands of Mediterranean regions? Water 10:1747. https://doi.org/10.3390/w10121747

Lu D, Weng Q (2006) Use of impervious surface in urban land-use classification. Remote Sens Environ 102(1–2):146–160

Lu D, Hetrick S, Moran E, Li G (2012) Application of time series Landsat images to examining land-use/land-cover dynamic change. Photogramm Eng Remote Sens 78(7):747

Malik A, Kumar A, Salih SQ, Kim S, Kim NW, Yaseen ZM, Singh VP (2020) Drought index prediction using advanced fuzzy logic model: regional case study over Kumaon in India. PLoS ONE 15(5):e0233280

Malik A, Kumar A, Kisi O, Khan N, Salih SQ, Yaseen ZM (2021) Analysis of dry and wet climate characteristics at Uttarakhand (India) using effective drought index. Nat Hazards 105(2):1643–1662

Mallick J, Bindajam AA, AlQadhi S, Ahmed M, Hang HT, Thanh NV (2020) A comparison of four land surface temperature retrieval method using TERRA-ASTER satellite images in the semi-arid region of Saudi Arabia. Geocarto Int 1–25. https://doi.org/10.1080/10106049.2020.1790675

Mallick J, Singh VP, Almesfer MK, Talukdar S, Alsubhi M, Ahmed M, Khan RA (2021) Spatio-temporal analysis and simulation of land cover changes and their impacts on land surface temperature in urban agglomeration of Bisha Watershed, Saudi Arabia. Geocarto Int 1–27. https://doi.org/10.1080/10106049.2021.1980616

Masoudi M (2021) Estimation of the spatial climate comfort distribution using tourism climate index (TCI) and inverse distance weighting (IDW)(case study: Fars Province, Iran). Arab J Geosci 14(5):1–13

Mehr AD, Akdegirmen O (2021) Estimation of urban imperviousness and its impacts on flashfloods in Gazipaşa. Turkey Knowledge-Based Eng Sci 2(1):9–17

Meshesha TW, Tripathi SK, Khare D (2016) Analyses of land use and land cover change dynamics using GIS and remote sensing during 1984 and 2015 in the Beressa Watershed Northern Central Highland of Ethiopia. Model Earth Syst Environ 2(4):1–12

Mutowo G & Chikodzi D. (2014). Remote sensing based drought monitoring in Zimbabwe. *Disaster Prevention and Management*.

Novotná M, Mikeš O, Komprdová K (2015) Development and comparison of regression models for the uptake of metals into various field crops. Environ Pollut 207:357–364. https://doi.org/10.1016/j.envpol.2015.09.043

Owojori A & Xie H. (2005, March). Landsat image-based LULC changes of San Antonio, Texas using advanced atmospheric correction and object-oriented image analysis approaches. In *5th international symposium on remote sensing of urban areas, Tempe, AZ*.

Patel NR, Anapashsha R, Kumar S, Saha SK, Dadhwal VK (2009) Assessing potential of MODIS derived temperature/vegetation condition index (TVDI) to infer soil moisture status. Int J Remote Sens 30(1):23–39

Pei F, Wu C, Liu X, Li X, Yang K, Zhou Y, ... & Xia G. (2018). Monitoring the vegetation activity in China using vegetation health indices. Agri Forest Meteorol 248, 215-227

Pramanik S, Punia M (2019) Assessment of green space cooling effects in dense urban landscape: a case study of Delhi, India. Modeling Earth Systems and Environment 5(3):867–884. https://doi.org/10.1007/s40808-019-00573-3

Pramanik S, Punia M (2020) Land use/land cover change and surface urban heat island intensity: source–sink landscape-based study in Delhi, India. Environ Dev Sustain 22(8):7331–7356

Potter BE, Teclaw RM, Zasada JC (2001) The impact of forest structure on near-ground temperatures during two years of constructing temperature extremes. Agric for Meteorol 106(4):331–336

Quiring SM, Ganesh S (2010) Evaluating the utility of the vegetation condition index (VCI) for monitoring meteorological drought in Texas. Agric for Meteorol 150(3):330–339

Qutbudin I, Shiru MS, Sharafati A, Ahmed K, Al-Ansari N, Yaseen ZM, ... & Wang X. (2019). Seasonal drought pattern changes due to climate variability: case study in Afghanistan. Water, 11(5), 1096

Ramachandra TV, Bharath HA, Vinay S (2013) Land use land cover dynamics in a rapidly urbanizing landscape. SCIT J 13:1–12

Rajeshwari A, Mani ND (2014) Estimation of land surface temperature of Dindigul district using Landsat 8 data. Int J Res Eng Technol 3(5):122–126

Rhee J, Im J, Carbone GJ (2010) Monitoring agricultural drought for arid and humid regions using multi-sensor remote sensing data. Remote Sens Environ 114(12):2875–2887

Rita A, Bonanomi G, Allevato E, Borghetti M, Cesarano G, Mogavero V, Rossi S, Saulino L, Zotti M, Saracino A (2021) Topography modulates near-ground microclimate in the Mediterranean Fagus sylvatica treeline. Sci Rep 11:8122. https://doi.org/10.1038/s41598-021-87661-6

Roy DP, Wulder MA, Loveland TR, Woodcock CE, Allen RG, Anderson MC, ... & Zhu Z. (2014). Landsat-8: Science and product vision for terrestrial global change research. Remote Sens Environ 145, 154-172. https://doi.org/10.1016/j.rse.2014.02.001

Sanikhani H, Kisi O, Maroufpoor E, Yaseen ZM (2019) Temperature-based modeling of reference evapotranspiration using several artificial intelligence models: application of different modeling scenarios. Theoret Appl Climatol 135(1):449–462

Sekertekin A, Bonafoni S (2020) Land surface temperature retrieval from Landsat 5, 7, and 8 over rural areas: Assessment of different retrieval algorithms and emissivity models and toolbox implementation. Remote Sens 12(2):294. https://doi.org/10.3390/rs12020294

Sejati AW, Buchori I, Rudiarto I (2019) The spatio-temporal trends of urban growth and surface urban heat islands over two decades in the Semarang Metropolitan Region. Sustain Cities Soc 46:101432

Shahabfar A, Ghulam A, Eitzinger J (2012) Drought monitoring in Iran using the perpendicular drought indices. Int J Appl Earth Obs Geoinf 18:119–127

Shen R, Huang A, Li B, Guo J (2019) Construction of a drought monitoring model using deep learning based on multi-source remote sensing data. Int J Appl Earth Obs Geoinf 79:48–57

Singh RP, Roy S, Kogan F (2003) Vegetation and temperature condition indices from NOAA AVHRR data for drought monitoring over India. Int J Remote Sens 24(22):4393–4402

Singh P, Kikon N, Verma P (2017) Impact of land use change and urbanization on urban heat island in Lucknow city, Central India. A remote sensing based estimate. Sustain Cities Soc 32:100–114

Sobrino JA, Irakulis I (2020) A methodology for comparing the surface urban heat island in selected urban agglomerations around the world from sentinel-3 SLSTR data. Remote Sens 12(12):2052. https://doi.org/10.3390/RS12122052

Sobrino JA, Raissouni N, Li ZL (2001) A comparative study of land surface emissivity retrieval from NOAA data. Remote Sens Environ 75(2):256–266. https://doi.org/10.1016/S0034-4257(00)00171-1

Sobrino JA, Jiménez-Muñoz JC, Paolini L (2004) Land surface temperature retrieval from LANDSAT TM 5. Remote Sens Environ 90(4):434–440. https://doi.org/10.1016/j.rse.2004.02.003

Somvanshi SS, Bhalla O, Kunwar P, Singh M, Singh P (2020) Monitoring spatial LULC changes and its growth prediction based on statistical models and earth observation datasets of Gautam Budh Nagar, Uttar Pradesh, India. Environ Dev Sustain 22(2):1073–1091

Strzepek K, Yohe G, Neumann J, Boehlert B (2010) Characterizing changes in drought risk for the United States from climate change. Environ Res Lett 5(4):044012

Su Z, Yacob A, Wen J, Roerink G, He Y, Gao B ... & van Diepen C. (2003). Assessing relative soil moisture with remote sensing data: theory, experimental validation, and application to drought monitoring over the North China Plain. Phys Chem Earth, Parts A/B/C, 28(1-3), 89-101

Su Z, He Y, Dong X & Wang L. (2017). Drought monitoring and assessment using remote sensing. In *Remote Sens Hydrol Extremes* (pp. 151–172). Springer, Cham.

Sur C, Park SY, Kim TW & Lee JH. (2019). Remote sensing-based agricultural drought monitoring using hydrometeorological variables. *KSCE J Civil Engi*

Szewczak K, Łoś H, Pudełko R, Doroszewski A, Gluba Ł, Łukowski M, ... & Usowicz B. (2020). Agricultural drought monitoring by MODIS potential evapotranspiration remote sensing data application. Remote Sens 12(20), 3411

Tabari H, Marofi S, Aeini A, Talaee PH, Mohammadi K (2011) Trend analysis of reference evapotranspiration in the western half of Iran. Agric for Meteorol 151(2):128–136

Tao H, Liao X, Li Y, Xu C, Zhu G, Cassidy DP (2020) Quantifying influences of interacting anthropogenic-natural factors on trace element accumulation and pollution risk in karst soil. Sci Total Environ 721:137770. https://doi.org/10.1016/j.scitotenv.2020.137770

Tepanosyan G, Muradyan V, Hovsepyan A, Pinigin G, Medvedev A, Asmaryan S (2021) Studying spatial-temporal changes and relationship of land cover and surface Urban Heat Island derived through remote sensing in Yerevan. Armenia Build Environ 187:107390

Tolba MKS & Najib W. (2009). Arab environment: climate change: impact of climate change on Arab countries. Arab Forum for Environ Develop (AFED).

Voogt JA, Oke TR (2003) Thermal remote sensing of urban climates. Remote Sens Environ 86(3):370–384

Wang PX, Li XW, Gong JY & Song C. (2001). Vegetation temperature condition index and its application for drought monitoring. In *IGARSS 2001. Scanning the Present and Resolving the Future. Proceedings. IEEE 2001 International Geoscience and Remote Sensing Symposium (Cat. No. 01CH37217)* (Vol. 1, pp. 141–143). IEEE.

Wang L, Wang P, Li L, Xun L, Kong Q, Liang S (2018) Developing an integrated indicator for monitoring maize growth condition using remotely sensed vegetation temperature condition index and leaf area index. Comput Electron Agric 152:340–349

Weng Q, Lu D, Schubring J (2004) Estimation of land surface temperature–vegetation abundance relationship for urban heat island studies. Remote Sens Environ 89(4):467–483. https://doi.org/10.1016/j.rse.2003.11.005

West H, Quinn N, Horswell M (2019) Remote sensing for drought monitoring & impact assessment: Progress, past challenges and future opportunities. Remote Sens Environ 232:111291

Xu X, Du Z, Zhang H (2016) Integrating the system dynamic and cellular automata models to predict land use and land cover change. Int J Appl Earth Obs Geoinf 52:568–579

Yu X, Guo X, Wu Z (2014) Land surface temperature retrieval from Landsat 8 TIRS—Comparison between radiative transfer equation-based method, split window algorithm and single channel method. Remote Sens 6(10):9829–9852

Zhang Y, Liu X, Jiao W, Zeng X, Xing X, Zhang L, ... & Hong Y. (2021). Drought monitoring based on a new combined remote sensing index across the transitional area between humid and arid regions in China. Atmospheric Res 264, 105850

Zhou X, Wang P, Tansey K, Zhang S, Li H, Wang L (2020) Developing a fused vegetation temperature condition index for drought monitoring at field scales using Sentinel-2 and MODIS imagery. Comput Electron Agric 168:105144

Zoungrana BJ, Conrad C, Thiel M, Amekudzi LK, Da ED (2018) MODIS NDVI trends and fractional land cover change for improved assessments of vegetation degradation in Burkina Faso, West Africa. J Arid Environ 153:66–75

Publisher's note Springer Nature remains neutral with regard to jurisdictional claims in published maps and institutional affiliations.